Structural compression and vibrational properties of $Bi_{12}SiO_{20}$ sillenite from experiment and theory



2010 J. Phys.: Condens. Matter 22 505401

(http://iopscience.iop.org/0953-8984/22/50/505401)

J. Phys.: Condens. Matter **22** (2010) 505401 (16pp) doi:10.1088/0953-8984/22/50/505401

# Structural compression and vibrational properties of $Bi_{12}SiO_{20}$ sillenite from experiment and theory

**Leonore Wiehl[1,6], Alexandra Friedrich[1], Eiken Haussühl[1], Wolfgang Morgenroth[1,2], Andrzej Grzechnik[3], Karen Friese[3], Björn Winkler[1], Keith Refson[4] and Victor Milman[5]**

[1] Institut für Geowissenschaften, Goethe Universität Frankfurt, Altenhöferallee 1, D-60438 Frankfurt a.M., Germany
[2] c/o DESY/HASYLAB, D-22603 Hamburg, Germany
[3] Departamento Física Materia Condensada, Facultad de Ciencia y Tecnología, Universidad del País Vasco, Apartado 644, E-48080 Bilbao, Spain
[4] Rutherford Appleton Laboratories, Chilton, Didcot, Oxfordshire OX11 0QX, UK
[5] Accelrys Ltd, 334 Science Park, Cambridge CB4 0WN, UK

E-mail: L.Wiehl@kristall.uni-frankfurt.de

Received 28 September 2010, in final form 5 November 2010
Published 26 November 2010
Online at stacks.iop.org/JPhysCM/22/505401

**Abstract**

The crystal structure of the bismuth silicon oxide $Bi_{12}SiO_{20}$ was determined by single-crystal x-ray diffraction at ambient conditions and at high pressure. Single-crystal intensity data between 0.0001 and 16.8(3) GPa were collected in house with Mo K$\alpha$ radiation and with synchrotron radiation ($\lambda = 0.45$ Å) at HASYLAB (D3), while lattice parameters were measured up to 23.0(3) GPa. The large cavities which exist in the crystal structure and host the lone electron pairs of the $Bi^{3+}$ ions are considerably compressed at high pressure. The crystal structure, however, remains stable and the lone electron pair is stereochemically active up to at least 16.8 GPa. A larger compression in the direction of the lone electron pairs by shear deformation was not observed. Raman spectra of $Bi_{12}SiO_{20}$ were measured on powder samples during pressure decrease from 39.1(1) GPa down to ambient pressure and on single crystals during pressure increase up to 12.50(3) GPa. Density functional perturbation theory was used to compute Raman frequencies and intensities at ambient pressure and to investigate pressure-induced changes up to 50 GPa.

(Some figures in this article are in colour only in the electronic version)

S Online supplementary data available from stacks.iop.org/JPhysCM/22/505401/mmedia

## 1. Introduction

Sillenites are non-centrosymmetric oxides with composition $Bi_{12}M_xO_{20\pm\delta}$ which crystallize in space group $I23$ (figure 1). $M$ represents elements of the second to 15th group of the periodic table and $x \leqslant 1$. Depending on the occupation of the tetrahedral $M^{n+}$ site, which may contain also $Bi^{3+}$ ions in the case of $n \neq 4$, vacancies or additional atoms in the oxygen sublattice ($\pm\delta$) are introduced for charge compensation. The prototype of all sillenites is the mineral 'sillenite', $\gamma$-$Bi_2O_3$ (Sillen 1938), which is metastable at ambient conditions (Wells 1984). The sillenite structure ($\gamma$-phase) can be stabilized at ambient conditions by addition of metal oxides in a ratio of $M$:Bi = 1:12. Up to now more than 60 sillenite compounds $Bi_2O_3$–$M_xO_y$ with $M^{n+}$ cations and numerous solid solutions thereof have been synthesized (Skorikov *et al* 2005). In the so-called 'stoichiometric sillenites' $M$ is tetravalent and the oxygen lattice is fully occupied ($x = 1$, $\delta = 0$). An important feature of the sillenite structure is the stereochemically active $6s^2$ lone electron pair (LEP) of

[6] Author to whom any correspondence should be addressed.

 

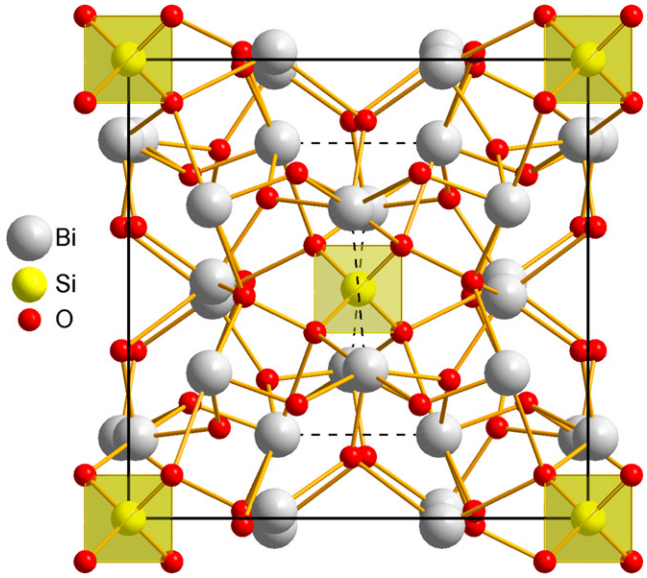


**Figure 1.** Crystal structure of the sillenite $Bi_{12}SiO_{20}$, space group $I23$. The $Bi^{3+}$ $6s^2$ lone electron pairs are oriented along the closest Bi–Bi contacts which are marked by dashed lines.

$Bi^{3+}$, which is, in combination with the lack of inversion symmetry, the source of outstanding electrical and optical properties. In particular, the photorefractive effect is used in many technical applications of sillenites (Baade *et al* 2001, Buse 1997, Georges *et al* 2001), and single crystals of sillenite also serve as optical sensors for electric current and voltage (van den Tempel 1993, Kaneko *et al* 1999, Filippov *et al* 2000) or as surface acoustic wave guides (Lu *et al* 2000).

The present study focuses on $Bi_{12}SiO_{20}$ (BSO), as BSO is considered to be a 'stoichiometric' sillenite. Nevertheless, the exact occupancy of the tetrahedral site has been discussed repeatedly for this compound. X-ray data on single crystals of BSO at ambient conditions were collected by Abrahams *et al* (1979) and neutron data by Neov *et al* (2002). In both cases the Si occupancy of the tetrahedral site was studied and could be refined. The result was a value of 0.99(6) (full occupancy) for neutron diffraction (Neov *et al* 2002), but only 0.87(8) for the x-ray measurements (Abrahams *et al* 1979). The crystal structure of BSO is composed of $SiO_4$ tetrahedra (site symmetry 23) and distorted $BiO_5\square$ octahedra (where $\square$ denotes an unoccupied position). The instability of the $\gamma$-$Bi_2O_3$ structure at ambient conditions is explained by the fact that $Bi^{3+}$ ions also occupy tetrahedral sites, which are much too small to accommodate the LEP. According to the model of Radaev *et al* (1992) only 80% of the tetrahedral sites in $\gamma$-$Bi_2O_3$ are filled with Bi. In these tetrahedra one of the corners is occupied by the LEP, resulting in an oxygen deficiency ($BiO_3\square$). The remaining 20% of tetrahedral sites in the structure are empty ($\square O_4$).

Sillenites have not been investigated at high pressure up to now. For pure $Bi_2O_3$ a high pressure phase has been synthesized at 6 GPa and 1150 K, which is isotypic to hexagonal $La_2O_3$ (Atou *et al* 1998). In this structure La shows a $1 + 3 + 3$ coordination with $1 + 3$ oxygen atoms forming a regular trigonal pyramid and three further oxygen atoms at longer distances, forming all together a capped trigonal antiprism. In the sillenite structure Bi shows a $5 + 2$ coordination with five oxygen atoms forming a distorted square pyramid and two other oxygen atoms at longer distances. Thus compression could induce a change in the coordination sphere around Bi leading to coordination polyhedra similar to the ones observed in the $La_2O_3$ structure type. The high symmetry of the sillenite structure, however, has to be taken into account in this consideration. There are 24 symmetrically equivalent Bi atoms in the unit cell with coordination polyhedra in different orientations, such that the $Bi^{3+}$ LEPs are oriented approximately in three different, mutually perpendicular directions. This opens the possibility that the anisotropic compression of the Bi coordination polyhedra might be 'frustrated' similar to the behaviour observed in $Bi_2Ti_2O_7$ pyrochlores (Seshadri 2006), where coherent off-centre movements of the $Bi^{3+}$ ions are frustrated due to the competing interactions in the highly symmetric cubic lattice.

Structural studies of several compounds containing LEPs under high pressure have shown that the influence of pressure leads to distinct phenomena and is difficult to predict. In general, the application of pressure leads to the reduction of the stereochemical activity of the LEP. Examples are bismuthinite, $Bi_2S_3$ (Lundegaard *et al* 2005), isostructural stibnite, $Sb_2S_3$ (Lundegaard *et al* 2003), and galenobismutite, $PbBi_2S_4$ (Olsen *et al* 2007). An extraordinary strong pressure effect resulting in the nearly complete loss of the stereochemical activity was detected in tetragonal $Pb_3O_4$ (Dinnebier *et al* 2003). The crystal structure is compressed mainly in the direction of the LEP and after two phase transitions at about 3 and 6 GPa changes into an orthorhombic phase, where the $Pb^{2+}$ $6s^2$ electron pair has a nearly pure *s*-character. In a density functional theory based study the pressure-induced delocalization of a LEP at 5 GPa was observed in $CsGeCl_3$ (Winkler *et al* 1998).

Pressure frequently induces structural phase transitions in LEP compounds, while stereoactivity still persists in the high-pressure structures. For example, $Bi_2Ga_4O_9$, which is characterized by the existence of different types of Ga–O and Bi–O coordination polyhedra, undergoes a structural phase transition at 16 GPa (Friedrich *et al* 2010) and the Bi coordination is increased from $4 + 2$ to $6 + 1$. Stereoactivity in this compound is still observed up to the highest pressure of 30.5 GPa reached in the study. Further examples are the two sulfosalts lillianite, $Pb_3Bi_2S_6$ (Olsen *et al* 2008), and heyrovskyite, $Pb_6Bi_2S_9$ (Olsen *et al* 2010). Here, first-order phase transitions are induced by pressure. Some of the bonds in the structures are broken, while others are newly formed leading to changes in the coordination numbers of the LEP cations. In $BiB_3O_6$ the first-order phase transition in the pressure range between 6.09 and 6.86 GPa (Dinnebier *et al* 2009) leads to an increase of the Bi coordination number from 6 to 8. An increase to coordination number 8 is also a consequence of the subsequent pressure-induced transitions in PbS: in the ambient pressure phase Pb is coordinated by 6 sulfur atoms, in the intermediate phase the coordination number is 7 and in the highest pressure polymorph 8 S atoms

**Table 1.** Experimental details of data collection and refinement of BSO, space group $I23$, $Z = 2$, with Mo K$\alpha$ radiation at ambient conditions (Xcalibur) and with synchrotron radiation at high pressure (HASYLAB).

| Pressure (GPa) | 0.0001 | 3.1(2) | 5.9(2) | 9.1(2) | 16.8(3) |
|---|---|---|---|---|---|
| $a$ (Å) | 10.1049(2) | 9.944(4) | 9.839(4) | 9.744(5) | 9.54(1) |
| $V$ (Å$^3$) | 1031.81(4) | 983.2(7) | 952.6(6) | 925.3(8) | 869(2) |
| $\varrho$ (g cm$^{-3}$) | 9.192 | 9.647 | 9.957 | 10.251 | 10.914 |
| $\mu$ (mm$^{-1}$) | 102.1 | 33.2 | 34.2 | 35.3 | 37.5 |
| X-ray source | Sealed tube | Synchrotron | Synchrotron | Synchrotron | Synchrotron |
| $\lambda$ (Å) | 0.710 73 | 0.45 | 0.45 | 0.45 | 0.45 |
| Detector | CCD | Point | Point | Point | Point |
| Standard reflections | None | 10 10 $\bar{1}0$ | 10 10 $\bar{1}0$ | 10 10 $\bar{1}0$ | 4 4 4 |
| | None | $\bar{1}0$ 10 10 | $\bar{1}0$ 10 10 | $\bar{1}0$ 10 10 | 2 $\bar{3}$ $\bar{1}$ |
| Measured reflections | 10 433 | 2728 | 2815 | 1806 | 1392 |
| Resolution (sin$\theta_{max}/\lambda$) (Å$^{-1}$) | 0.76 | 0.94 | 0.90 | 0.97 | 0.83 |
| $R$ (int) | 0.0611 | 0.0794 | 0.0945 | 0.0427 | 0.0482 |
| $R$ (sigma) | 0.0211 | 0.0431 | 0.0596 | 0.0260 | 0.0328 |
| Unique reflections (total) | 605 | 745 | 950 | 836 | 619 |
| Unique reflections ($I > 2\sigma(I)$) | 579 | 726 | 930 | 831 | 614 |
| Extinction coefficient | 0.001 27(6) | 0.0244(7) | 0.0219(8) | 0.0263(9) | 0.0005(2) |
| Refined parameters | 27 | 27 | 27 | 27 | 27 |
| $R1$ ($I > 2\sigma(I)$) | 0.0194 | 0.0243 | 0.0360 | 0.0221 | 0.0329 |
| $wR2$ (all) | 0.0413 | 0.0509 | 0.0741 | 0.0599 | 0.0798 |
| Goodness of fit | 1.065 | 1.063 | 1.063 | 1.167 | 1.082 |

$R1 = \sum ||F_o| - |F_c|| / \sum |F_o|$; $wR2 = \{\sum[w(F_o^2 - F_c^2)^2] / \sum[w(F_o^2)^2]\}^{1/2}$.

belong to the coordination sphere of Pb (Chattopadhyay *et al* 1986, Ahuja 2003, Grzechnik and Friese 2010).

Another effect of pressure on LEP-containing compounds is pressure-induced amorphization. Examples are $Bi_4M_3O_{12}$ ($M$: Si, Ge, Ti), which are built from $SiO_4$ tetrahedra and distorted trigonal antiprismatic $BiO_6$ units similar to those in $La_2O_3$, and are known to amorphize under pressures of approximately 8 GPa (Arora *et al* 2004, Meng *et al* 1998, Grzechnik 2009). However, it has been pointed out that the sillenites themselves are not expected to decompose (or amorphize) on compression, since the volume changes during the formation of BSO and BGO from the $Bi_2O_3$, $SiO_2$ and $GeO_2$ oxides are positive (Ravindran *et al* 2002, Arora *et al* 2004).

In this work we investigated the crystal structure of BSO at high pressure by *in situ* x-ray diffraction and the pressure evolution of vibrational properties by Raman spectroscopy in order to elucidate how the stereochemical activity of the LEP of $Bi^{3+}$ and the coordination sphere of Bi are affected by the application of high pressure. The experimental studies are complemented by density functional theory based atomistic model calculations.

## 2. Experimental details

### 2.1. Sample preparation

Crystals from two different sources were used.

Batch 1: several large crystals of BSO with optical quality and with sizes suitable for physical measurements (>cm$^3$) were bought from Vladimir L Tarasov (Gem minerals from Russia). Tiny pieces were cut from a large crystal and were used for the single-crystal x-ray diffraction experiments in Frankfurt (Xcalibur) and Hamburg (synchrotron at HASYLAB). A small portion of material was milled in an agate mortar and was used for Raman spectroscopy of a powder sample at high pressure in Frankfurt.

Batch 2: a second batch of single crystals of BSO, used in Bilbao for the x-ray measurements with the IPDS-2T diffractometer and for the single-crystal Raman measurements, was provided by V Marinova (Sofia). The crystals were grown by the Czochralski technique as described in Neov *et al* (2002). Crystals for the diffraction and spectroscopic measurements came from the same batch, but were different individuals.

### 2.2. Single-crystal x-ray diffraction at ambient conditions

Single-crystal intensity data were collected using an Xcalibur3 four-circle diffractometer from Oxford diffraction equipped with a Sapphire3 CCD camera and a sealed tube with Mo K$\alpha$ radiation. The crystal had dimensions of 85 × 45 × 30 $\mu$m$^3$. The sample-to-detector distance was 50 mm and a total of 845 exposures (1° crystal rotation per frame, 120 s exposure time) were collected. Data reduction and empirical absorption correction were performed with the program CrysAlis, version 1.171.33.36 (Oxford diffraction). The starting atomic positions were taken from the literature (Neov *et al* 2002) and the structure refinement was carried out with SHELXL97-2 (Sheldrick 1997). Anisotropic displacement parameters were refined for all atoms. An extinction correction was applied. Experimental details are included in table 1.[7]

### 2.3. Single-crystal x-ray diffraction at high pressure

Two sets of intensity data were collected at high pressure, one with Mo K$\alpha$ radiation and the other with synchrotron

[7] Further details of the crystallographic investigations can be obtained from the Fachinformationszentrum Karlsruhe, D-76344 Eggenstein-Leopoldshafen, Germany, on quoting the depository numbers CSD 422385–422389.

**Table 2.** Experimental details of data collection and refinement of BSO with Mo K$\alpha$ radiation ($\lambda = 0.710\,73$ Å) at high pressure (Stoe IPDS-2T).

| Pressure (GPa) | 2.27(3) | 3.25(3) | 4.17(3) | 5.23(3) | 6.18(3) |
|---|---|---|---|---|---|
| $a$ (Å) | 9.982(1) | 9.940(1) | 9.904(1) | 9.864(1) | 9.831(1) |
| $V$ (Å$^3$) | 994.61(2) | 982.2(2) | 971.4(2) | 959.8(2) | 950.1(2) |
| $\varrho$ (g cm$^{-3}$) | 9.536 | 9.656 | 9.763 | 9.882 | 9.982 |
| $\mu$ (mm$^{-1}$) | 105.9 | 107.2 | 108.4 | 109.7 | 110.8 |
| Measured reflections | 3194 | 3097 | 3089 | 3065 | 3021 |
| Resolution ($\sin\theta_{max}/\lambda$) (Å$^{-1}$) | 0.67 | 0.66 | 0.67 | 0.67 | 0.67 |
| $R$ (int) | 0.0885 | 0.0831 | 0.0806 | 0.0923 | 0.0812 |
| $R$ (sigma) | 0.0536 | 0.0506 | 0.0494 | 0.0480 | 0.0511 |
| Unique reflections (total) | 354 | 332 | 324 | 326 | 324 |
| Unique reflections ($I > 2\sigma(I)$) | 302 | 290 | 286 | 285 | 278 |
| Extinction coefficient | 0.28(3) | 0.28(3) | 0.26(3) | 0.28(3) | 0.29(3) |
| Refined parameters | 18 | 18 | 18 | 18 | 18 |
| $R1$ ($I > 2\sigma(I)$) | 0.0671 | 0.0566 | 0.0559 | 0.0545 | 0.0544 |
| $wR2$ (all) | 0.1435 | 0.1118 | 0.1014 | 0.1067 | 0.1000 |
| Goodness of fit | 2.85 | 2.53 | 2.37 | 2.44 | 2.30 |

$R1 = \sum ||F_o| - |F_c|| / \sum |F_o|$; $wR2 = \{\sum[w(F_o^2 - F_c^2)^2] / \sum[w(F_o^2)^2]\}^{1/2}$.

radiation. Ruby chips were loaded with the crystals for pressure determination by the laser-induced ruby-fluorescence technique (Piermarini *et al* 1975, Mao *et al* 1978, 1986). A 4:1 mixture of methanol and ethanol was used as pressure transmitting medium for the measurements below 10 GPa. For studies at pressures above 10 GPa compressed neon gas was loaded into the pressure chamber at a pressure of 0.2 GPa within a pressure vessel in Frankfurt.

One set of single-crystal intensity data was measured in a diamond anvil cell of the Boehler–Almax type (Boehler 2006) using a STOE diffractometer equipped with an image plate IPDS-2T with Mo K$\alpha$ radiation at pressures of 2.27(3), 3.25(3), 4.17(3), 5.23(3) and 6.18(3) GPa. A stainless steel gasket of 250 $\mu$m was pre-indented to a thickness of 80 $\mu$m. The size of the hole in the gasket was 250 $\mu$m, the culets of the diamonds were 600 $\mu$m. A single crystal of size $60 \times 60 \times 20$ $\mu$m$^3$ with excellent quality was chosen for the high pressure experiments. Measurements were carried out with the image plate in two different $\theta$ positions (0° and 15°). The diffracted intensities were indexed and integrated using the STOE software (STOE and CIE GmbH 2006). Areas of the images shaded by the diamond anvil cell were masked prior to integration. Three orientation matrices corresponding to the sample and the two diamond crystals were simultaneously used in the integration and sample reflections which overlapped with diamond reflections were excluded. The corrections for the effects of absorption by the diamond anvils and the crystal were made using the program ABSORB (Angel 2004) and the STOE software (STOE and CIE GmbH 2006), respectively. Data were refined using the program JANA2006 (Petricek *et al* 2006) with starting coordinates from Neov *et al* (2002). Only the displacement parameters of the heavy atoms were treated anisotropically. In addition, as the isotropic displacement parameters of the oxygen atoms were identical within their standard deviations, they were restricted to be equal. The introduction of this restriction had no significant influence on the overall agreement factors. An isotropic extinction correction was applied (Coppens 1970). At all pressures, an inversion twin model was tested, which did not lead to a significant volume fraction for the second twin individual at any of the pressure points. Details of data collection, atomic positions and interatomic distances and angles are given in tables 2–5.

For the measurements with synchrotron radiation, pressures were generated with ETH-type and Boehler–Almax-type diamond anvil cells (DACs), all of them equipped with tungsten carbide seats and conical diamond anvils (Miletich *et al* 2000, Boehler and de Hantsetter 2004, Boehler 2006). The culet diameters varied between 370 and 600 $\mu$m and the x-ray apertures were about 80°. Up to pressures of 9 GPa the diameter of the pressure chamber was 260 $\mu$m within a steel (1.4310) gasket (pre-indented to a thickness of about 91 $\mu$m) and a single crystal of size $120 \times 88 \times 40$ $\mu$m$^3$ was loaded together with ruby chips. At pressures above 10 GPa the sample chamber was a hole of 165 $\mu$m in diameter in a tungsten gasket of 200 $\mu$m initial thickness, which had been pre-indented to a thickness of 48 $\mu$m. A single crystal of size $60 \times 57 \times 20$ $\mu$m$^3$ was loaded into the hole. The orientation matrix was determined at the loading pressure with the same in-house four-circle diffractometer as described in section 2.2 using a CCD camera in order to check for possible phase transitions and to save time in starting the experiment with the point detector at HASYLAB. Intensity data sets were collected at 3.1(2), 5.9(2), 9.1(2) and 16.8(3) GPa with synchrotron radiation at HASYLAB (beamline D3), Hamburg, Germany. Data were collected with a NaI scintillation detector, using a Huber four-circle diffractometer with Eulerian cradle in fixed phi ($\phi = 0$) geometry. The synchrotron radiation wavelength was 0.45 Å from a Si(111) double-crystal monochromator. The reflections were measured in step scan mode with 71 steps of width $\Delta\omega = 0.002°$ (3.1, 5.9, 9.1 GPa) and $\Delta\omega = 0.03°$ at 16.8 GPa. The extinct reflections due to the body centring were tested and, as none of them were observed with intensities $>1\sigma$, they were subsequently excluded from data collection. In a small range of the reciprocal space ($2\theta = 30°$–$32°$) all equivalent reflections were measured. For other $2\theta$-values care was taken to select at least all unique reflections of crystal class 23, which are well covered by an octant of, e.g., all positive

**Table 3.** Atom positions and equivalent isotropic displacement parameters (Å$^2$) of BSO crystals from batch 2 (Stoe IPDS-2T) and from batch 1 (Xcalibur and HASYLAB).

| Pressure (GPa) | 2.27(3) | 3.25(3) | 4.17(3) | 5.23(3) | 6.18(3) |
|---|---|---|---|---|---|
| Bi $x$ | 0.8256(2) | 0.8262(2) | 0.8266(2) | 0.8271(2) | 0.8275(2) |
| Bi $y$ | 0.6819(2) | 0.6816(2) | 0.6811(1) | 0.6808(2) | 0.6805(1) |
| Bi $z$ | 0.9851(2) | 0.9856(2) | 0.9857(1) | 0.9861(1) | 0.9864(1) |
| Bi $U_{equ}$ | 0.0168(6) | 0.0170(6) | 0.0154(5) | 0.0191(5) | 0.0166(5) |
| Si $x = y = z$ | 1.0000 | 1.0000 | 1.0000 | 1.0000 | 1.0000 |
| Si $U_{equ}$ | 0.020(6) | 0.013(5) | 0.008(4) | 0.017(5) | 0.011(4) |
| O1 $x$ | 0.872(3) | 0.870(3) | 0.870(2) | 0.871(3) | 0.866(2) |
| O1 $y$ | 0.744(3) | 0.745(3) | 0.743(3) | 0.741(3) | 0.740(3) |
| O1 $z$ | 0.516(3) | 0.520(3) | 0.518(3) | 0.515(4) | 0.512(3) |
| O1 $U_{equ}$ | 0.014(5) | 0.018(5) | 0.017(5) | 0.024(5) | 0.020(5) |
| O2 $x = y = z$ | 0.799(3) | 0.799(3) | 0.799(2) | 0.797(3) | 0.798(3) |
| O2 $U_{equ}$ | 0.014(5) | 0.018(5) | 0.017(5) | 0.024(5) | 0.020(5) |
| O3 $x = y = z$ | 0.089(3) | 0.094(3) | 0.099(3) | 0.097(3) | 0.099(3) |
| O3 $U_{equ}$ | 0.014(5) | 0.018(5) | 0.017(5) | 0.024(5) | 0.020(5) |
| Pressure (GPa) | 0.0001 | 3.1(2) | 5.9(2) | 9.1(2) | 16.8(3) |
| Bi $x$ | 0.82434(2) | 0.82612(2) | 0.82718(2) | 0.82818(2) | 0.82968(4) |
| Bi $y$ | 0.68251(2) | 0.68131(2) | 0.68045(2) | 0.67958(2) | 0.67773(4) |
| Bi $z$ | 0.98415(3) | 0.98571(2) | 0.98660(3) | 0.98739(2) | 0.98865(4) |
| Bi $U_{equ}$ | 0.00954(9) | 0.00751(8) | 0.0068(1) | 0.00613(8) | 0.0062(1) |
| Si $x = y = z$ | 1.0000 | 1.0000 | 1.0000 | 1.0000 | 1.0000 |
| Si $U_{equ}$ | 0.005(1) | 0.0064(8) | 0.0055(9) | 0.0033(8) | 0.004(2) |
| O1 $x$ | 0.8661(5) | 0.8662(4) | 0.8659(5) | 0.8663(5) | 0.8667(9) |
| O1 $y$ | 0.7476(5) | 0.7430(5) | 0.7408(6) | 0.7373(6) | 0.730(1) |
| O1 $z$ | 0.5146(5) | 0.5148(4) | 0.5133(5) | 0.5126(6) | 0.511(1) |
| O1 $U_{equ}$ | 0.0101(9) | 0.0099(6) | 0.0088(7) | 0.0084(8) | 0.010(1) |
| O2 $x = y = z$ | 0.8034(5) | 0.8020(5) | 0.8030(6) | 0.8000(6) | 0.795(1) |
| O2 $U_{equ}$ | 0.011(2) | 0.010(1) | 0.009(1) | 0.008(1) | 0.008(3) |
| O3 $x = y = z$ | 0.0936(5) | 0.0950(5) | 0.0959(6) | 0.0970(7) | 0.0982(9) |
| O3 $U_{equ}$ | 0.015(2) | 0.013(1) | 0.011(1) | 0.0010(2) | 0.008(3) |

Miller indices (*ppp*) and their Friedel mates (*nnn*). This choice includes already equivalent reflections due to one of the three-fold axes. Equivalent reflections due to two-fold axes were added by reflection groups of, e.g., (*pnn*) and (*npp*). The choice of the particular octants depended on the orientation of the crystal within the DAC.

Integrated intensity data were obtained using the beamline-adopted software REDUCE (Eichhorn 1987) and AVSORT (Eichhorn 1978). The absorption of the x-ray beam by the diamond anvils and by the crystal was corrected with the program ABSORB, version 6.1 (Angel 2004). Structure refinements were performed with SHELXL97-2 (Sheldrick 1997). The starting parameters for the refinements were taken from the results at ambient conditions. Extinction corrections were applied. Due to the geometrical constraints of a DAC and the reduced access of reciprocal space in the direction of the DAC axis (Miletich *et al* 2000) in high pressure experiments, anisotropic displacement parameters (ADPs) are expected to suffer from systematic errors in crystals with low symmetry. In cubic crystals, however, the high symmetry partly compensates these effects and therefore it is possible to refine ADPs. Moreover the refinement of ADPs can be justified by the quality and the number of measured data with 614–930 unique reflections ($I > 2\sigma(I)$) to fit only 27 parameters. Experimental details of the data collections are summarized in table 1. Atomic coordinates and the equivalent isotropic displacement parameters are given in table 3, whereas the anisotropic displacement parameters can be found in supplementary tables (available at stacks.iop.org/JPhysCM/22/505401/mmedia).

Up to 9.1 GPa, the crystals exhibited very sharp diffraction profiles with FWHMs of 0.015°–0.02°, which broadened, however, to FWHMs of 0.2°–0.3° at 16.8 GPa. This effect is probably due to the influence of the compressed neon gas, which freezes at 4.8 GPa and starts to deviate from hydrostatic conditions at 15 GPa (Klotz *et al* 2009). This broadening is also reflected in the increased standard deviation of the lattice parameter at 16.8 GPa due to a slight spread of the experimentally determined triclinic lattice constants and deviation of the lattice angles from 90° by up to 0.38°. In contrast, the triclinic lattice parameters determined below 10 GPa corresponded to cubic symmetry within the limits of error (less than $5 \times 10^{-4}$). After the subsequent pressure increase to 23.0(4) GPa the diffraction profiles degraded and had total widths of about 1.5°–2°. As a consequence, only unit cell parameters could be determined at this pressure, which showed a significant deviation from cubic symmetry ($a = 9.40(1)$ to 9.465(6) Å, $\alpha = 89.3(1)°$ to 90.14(8)°, $V = 837(4)$ Å$^3$). A possible explanation for these observations is that the crystal was clamped between the two diamonds at 23 GPa.

**Table 4.** Inter-atomic distances (Å) of BSO crystals from batch 2 (Stoe IPDS-2T) and from batch 1 (Xcalibur and HASYLAB) at different pressures.

| Pressure (GPa) | 2.27(3) | 3.25(3) | 4.17(3) | 5.23(3) | 6.18(3) |
|---|---|---|---|---|---|
| Si–O3(f) | 1.53(3) | 1.62(3) | 1.70(3) | 1.65(3) | 1.68(3) |
| Bi–O1(a) | 2.12(3) | 2.11(3) | 2.11(2) | 2.12(3) | 2.07(2) |
| Bi–O2 | 2.21(3) | 2.21(3) | 2.21(2) | 2.21(3) | 2.20(2) |
| Bi–O1(b) | 2.16(3) | 2.13(3) | 2.15(3) | 2.17(3) | 2.21(3) |
| Bi–O1(c) | 2.57(3) | 2.59(3) | 2.58(3) | 2.53(3) | 2.54(3) |
| Bi–O3(f) | 2.65(3) | 2.60(3) | 2.56(3) | 2.57(3) | 2.54(3) |
| Bi–O1(d) | 3.03(3) | 3.04(3) | 2.99(3) | 2.95(3) | 2.90(3) |
| Bi–O1(e) | 3.08(3) | 3.04(3) | 3.01(3) | 3.00(3) | 2.98(3) |
| Bi–Bi(g) | 3.494(3) | 3.468(2) | 3.445(2) | 3.423(2) | 3.402(2) |
| Bi–Bi(h) | 3.644(3) | 3.622(2) | 3.598(2) | 3.577(2) | 3.558(2) |
| Bi–Bi(i) | 3.672(3) | 3.661(2) | 3.650(2) | 3.638(2) | 3.629(2) |
| Bi–Bi(j) | 3.708(2) | 3.703(2) | 3.696(2) | 3.689(2) | 3.684(2) |
| Pressure (GPa) | 0.0001 | 3.1(2) | 5.9(2) | 9.1(2) | 16.8(3) |
| Si–O3(f) | 1.638(9) | 1.637(9) | 1.63(1) | 1.64(1) | 1.62(2) |
| Bi–O1(a) | 2.073(5) | 2.075(4) | 2.068(6) | 2.076(5) | 2.081(9) |
| Bi–O2 | 2.208(2) | 2.199(2) | 2.185(2) | 2.188(3) | 2.184(5) |
| Bi–O1(b) | 2.214(5) | 2.200(4) | 2.200(5) | 2.197(6) | 2.18(1) |
| Bi–O1(c) | 2.618(5) | 2.579(4) | 2.542(5) | 2.515(6) | 2.46(1) |
| Bi–O3(f) | 2.651(4) | 2.597(4) | 2.564(4) | 2.532(5) | 2.478(7) |
| Bi–O1(d) | 3.069(5) | 2.986(5) | 2.927(6) | 2.867(6) | 2.75(1) |
| Bi–O1(e) | 3.159(5) | 3.045(5) | 2.988(6) | 2.922(6) | 2.79(1) |
| Bi–Bi(g) | 3.5644(5) | 3.470(1) | 3.411(1) | 3.358(2) | 3.258(2) |
| Bi–Bi(h) | 3.7023(5) | 3.617(1) | 3.561(1) | 3.508(2) | 3.399(2) |
| Bi–Bi(i) | 3.7068(3) | 3.661(1) | 3.630(1) | 3.601(2) | 3.534(2) |
| Bi–Bi(j) | 3.7353(5) | 3.709(2) | 3.690(2) | 3.674(2) | 3.634(2) |

Equivalent positions are: (a) $1.5 - x, 1.5 - y, 0.5 + z$; (b) $y, z, x$; (c) $y, 1 - z, 2 - x$; (d) $z + 1/2, -x + 1.5, -y + 1.5$; (e) $-z + 1.5, -x + 1.5, y + 1/2$; (f) $1 - z, 1 - x, 1 + y$; (g) $2 - x, y, 2 - z$; (h) $x, 1 - y, 2 - z$; (i) $-y + 1.5, z - 1/2, -x + 1.5$; (j) $z, x, y$.

### *2.4. High pressure Raman spectroscopy*

Micro-Raman measurements were performed both on single crystals and powder samples.

Raman spectra in the range 150–1000 $cm^{-1}$ were measured on compression from a single crystal of batch 2 in a diamond anvil cell of the DXR-6 type using an inVia Renishaw spectrometer equipped with an $Ar^+$ ion laser (514.5 nm) (figure 2). Caesium iodide was used as a pressure medium. The laser power was less than 100 mW. No damage to the crystal was visible during measurements. The crystals were not oriented for the Raman measurements as it is not possible to measure polarized spectra in a diamond anvil cell.

Raman spectra of a fine-grained powder sample from batch 1 were measured in 180° reflection geometry with a Renishaw Raman spectrometer (RM-1000) equipped with a Nd/YAG laser (532 nm, 200 mW) (figure 2). The system was calibrated using the band at 519 $cm^{-1}$ of a silicon wafer (Temple and Hathaway 1973). We employed a 20× objective lens with a long working distance. The sample was loaded in a Boehler–Almax DAC with neon gas as pressure medium and has been used for other experiments on pressure increase before. In the Raman measurements the pressure was reduced from 39.1(1) GPa in steps of about 2–5 GPa and at each point a spectrum was recorded in the range from 100 to 1000 $cm^{-1}$ with an exposure time of 600 s and 100% laser power. All spectra were corrected by subtracting a background and fitted to Lorentzian functions using the program DatLab (Syassen 2005).

Sillenites are sensitive to intense light, where the reported damage energy levels vary considerably (Li *et al* 2007). As the background resulting from the diamonds and/or neon gas was high, some damage of the powder sample, which showed only weak Raman signals, by the laser beam was unavoidable. This is indicated by the continuously decreasing intensity of the Raman signal between 39.1 and 26.5 GPa. On change of the measurement position at 22.2 GPa the peak to noise ratio increased. During measurements at further pressure decrease the intensity of the Raman lines weakened considerably and at ambient conditions (measured without the upper diamond and with only 2 mW laser power) only two broad lines at about 120 and 310 $cm^{-1}$ were observed instead of the typical sillenite spectrum.

### *2.5. DFT calculations*

In order to further investigate the pressure dependence of the observed Raman bands, variational density functional perturbation theory (DFPT) calculations were performed employing the CASTEP code (Clark *et al* 2005, Refson *et al* 2006). The code is an implementation of Kohn–Sham DFT based on a plane-wave basis set in conjunction with pseudopotentials. The plane-wave basis set is unbiased (as it is not atom-centred) and does not suffer from the

**Table 5.** Selected inter-atomic angles (deg) of BSO crystals from batch 2 (Stoe IPDS-2T) and from batch 1 (Xcalibur and HASYLAB) at different pressures.

| Pressure (GPa) | 2.27(3) | 3.25(3) | 4.17(3) | 5.23(3) | 6.18(3) |
|---|---|---|---|---|---|
| O1(a)–Bi–O2 | 80(1) | 81(1) | 80(1) | 79(1) | 77(1) |
| O1(a)–Bi–O1(b) | 90(1) | 90(1) | 90(1) | 89(1) | 90(1) |
| O1(a)–Bi–O1(c) | 84(1) | 84(1) | 83.8(9) | 84(1) | 84(1) |
| O1(a)–Bi–O3(f) | 87(1) | 85(1) | 84(1) | 84(1) | 83(1) |
| O1(b)–Bi–O1(c) | 66(1) | 66(1) | 66.1(9) | 66(1) | 67.4(8) |
| O1(b)–Bi–O2 | 85(1) | 84(1) | 84.2(9) | 84(1) | 84(1) |
| O3(f)–Bi–O2 | 85(1) | 86.3(9) | 87.5(9) | 87(1) | 87.5(9) |
| O3(f)–Bi–O1(c) | 123(1) | 122.0(9) | 120.1(9) | 120.9(9) | 119.0(9) |
| O1(d)–Bi–O1(e) | 106.5(9) | 107.0(8) | 106.6(8) | 106.3(9) | 106.5(8) |
| Bi–O1–Bi(h) | 100(1) | 100(1) | 98.9(9) | 99(10) | 96.8(9) |
| Bi–O1–Bi(i) | 118(1) | 119(1) | 118(1) | 116(1) | 116(1) |
| Bi–O2–Bi(j) | 114(1) | 114(1) | 114(1) | 113(1) | 114(1) |
| Bi–O3–Bi(k) | 101(1) | 103(1) | 105(1) | 104(1) | 105(1) |
| Bi–O3–Si | 117(2) | 116(2) | 114(1) | 115(2) | 114(1) |
| Pressure (GPa) | 0.0001 | 3.1(2) | 5.9(2) | 9.1(2) | 16.8(3) |
| O1(a)–Bi–O2 | 81.1(2) | 79.5(1) | 78.4(2) | 77.0(2) | 74.7(3) |
| O1(a)–Bi–O1(b) | 90.91(7) | 90.12(7) | 89.65(8) | 89.11(8) | 88.3(1) |
| O1(a)–Bi–O1(c) | 84.17(4) | 84.23(3) | 84.34(4) | 84.38(4) | 84.48(7) |
| O1(a)–Bi–O3(f) | 86.4(2) | 84.8(2) | 84.1(2) | 83.0(2) | 80.9(3) |
| O1(b)–Bi–O1(c) | 68.0(2) | 67.6(2) | 67.6(2) | 67.1(2) | 66.3(4) |
| O1(b)–Bi–O2 | 86.8(2) | 85.5(2) | 85.6(3) | 84.2(3) | 81.9(5) |
| O3(f)–Bi–O2 | 84.4(2) | 85.0(2) | 84.6(3) | 85.8(3) | 87.4(5) |
| O3(f)–Bi–O1(c) | 120.0(2) | 120.3(2) | 120.2(2) | 120.2(2) | 120.2(4) |
| O1(d)–Bi–O1(e) | 107.2(1) | 106.8(1) | 106.7(2) | 106.2(1) | 105.2(2) |
| Bi–O1–Bi(h) | 99.7(2) | 98.1(2) | 97.1(2) | 96.0(2) | 93.8(3) |
| Bi–O1–Bi(i) | 119.6(2) | 117.8(2) | 116.5(3) | 114.9(3) | 111.9(4) |
| Bi–O2–Bi(j) | 115.6(2) | 115.0(2) | 115.2(2) | 114.2(2) | 112.6(4) |
| Bi–O3–Bi(k) | 102.7(2) | 103.1(2) | 103.3(2) | 103.7(3) | 104.0(4) |
| Bi–O3–Si | 115.6(2) | 115.3(2) | 115.1(2) | 114.8(2) | 114.5(3) |

problem of basis-set superposition error unlike atom-centred basis sets. It also makes converged results straightforward to obtain in practice, as the convergence is controlled by a single adjustable parameter, the plane-wave cut-off, which we set to 990 eV. All pseudopotentials were norm-conserving. The local density approximation was used throughout. The Brillouin-zone integrals were performed using Monkhorst–Pack grids (Monkhorst and Pack 1976) with spacings between grid points of less than 0.028 $Å^{-1}$. A simultaneous optimization of the unit cell parameters and internal coordinates was performed so that forces were converged to 0.01 eV $Å^{-1}$ and the stress residual to 0.02 GPa.

Full geometry relaxations were performed for the BSO crystal structure at six pressures in the interval between 0 and 50 GPa. Raman activities were computed using a hybrid method combining density functional perturbation theory with finite displacements. The Raman activity tensor of a mode is given by the derivative of the dielectric permittivity tensor with respect to the mode amplitude. This was evaluated using a numerical central difference approximation between permittivity tensors computed using DFPT at geometries displaced from equilibrium by small positive and negative amplitudes according to the mode eigenvector. This method is similar to that of Porezag and Pederson (1996) except for our use of DFPT to compute the dielectric permittivity. A simulated Raman spectrum at 0 GPa is shown in figure 3.

## 3. Results and discussion

### *3.1. Compressibility*

The relative unit cell volume of BSO as a function of pressure (cf table 1) is shown in figure 4. A Birch–Murnaghan equation of state (EoS) up to third order (Birch 1947) was fitted to the data using the program EOS–FIT (Angel 2001), and resulted in the bulk modulus $B_0 = 63(4)$ GPa with pressure derivative $B' = 5.6(5)$. This result is in agreement with the value of $B_0 = 63.08(2)$ GPa deduced from ultrasonic measurements of the elastic constants of BSO at ambient conditions (Gospodinov *et al* 1988) and the pressure derivative $B' = 7.6(2)$ derived from piezo-elastic constants at 0.2 GPa. For the DFT calculations up to 50 GPa the corresponding EoS-fit resulted in $B_0 = 78(1)$ GPa and $B' = 4.94(7)$. DFT–LDA calculations typically overestimate the bulk modulus and this is also the case in the present study.

The crystal structure remains stable without any phase transition at least up to 23 GPa. The compressibility of BSO is lower than the one observed for $Bi_4Ge_3O_{12}$ ($B_0 = 48(2)$ GPa, $B' = 9(1)$ (Meng *et al* 1998, Arora *et al* 2004)), but much higher than that of the ternary bismuth oxides related to the mullite family. $Bi_2Ga_4O_9$, which undergoes a structural phase transition at about 16 GPa (Friedrich *et al* 2010), has bulk moduli of $B_0 = 102(8)$ GPa ($B' = 3.8(2)$) in the low

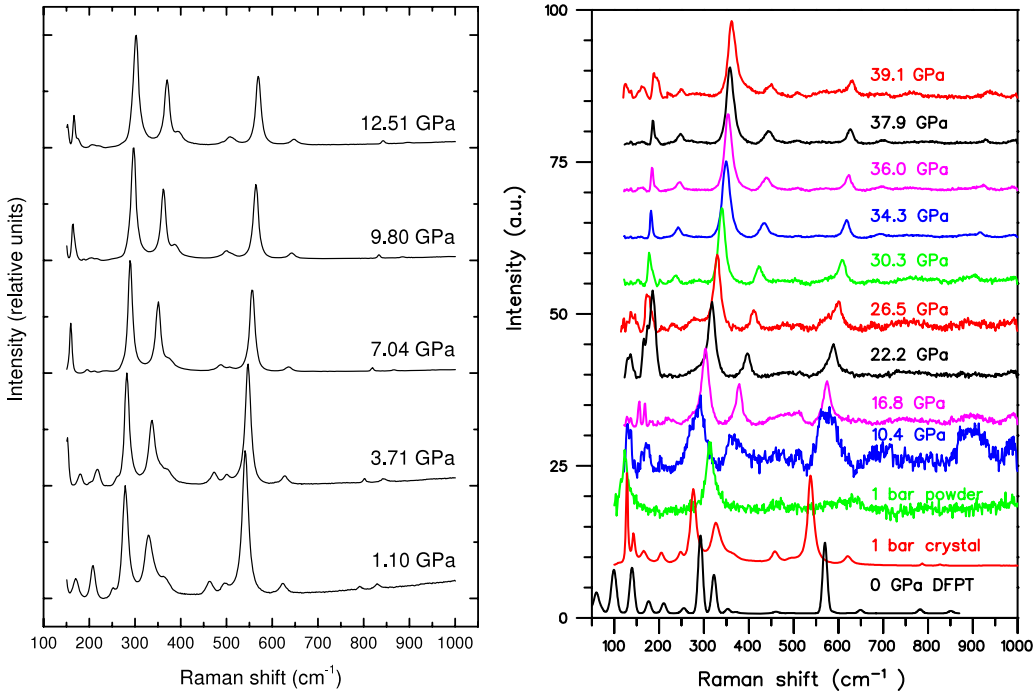


**Figure 2.** Left: selected Raman spectra of single crystals at different pressures. Right: Raman spectra of a powder sample at high pressures. The background was subtracted and the intensity scaled to a common level. Included are two further spectra, one measured from a single crystal at 1 bar as reference and the other one calculated with DFPT at 0 GPa.

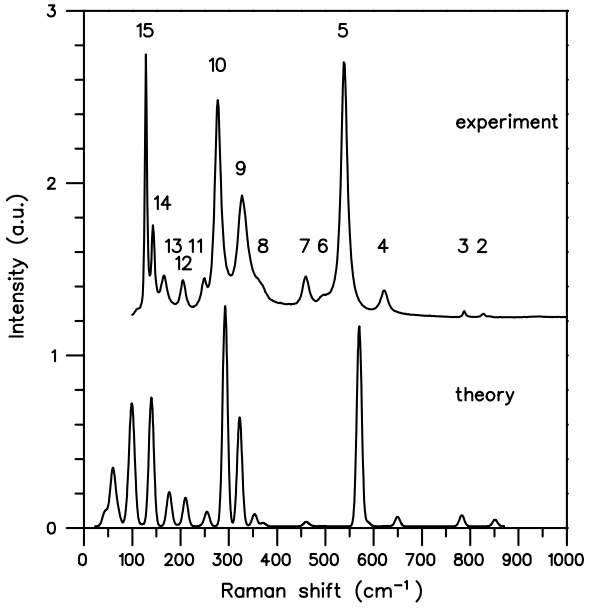


**Figure 3.** Simulated Raman spectrum at 0 GPa in comparison to the observed one with numbering scheme of the modes.

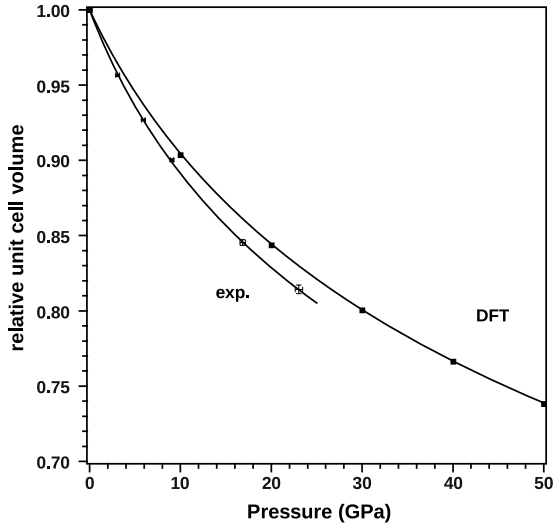


**Figure 4.** Pressure dependence of the relative unit cell volume of BSO from experiment and theory. The solid lines represent the third-order Birch–Murnaghan equations of state, which were fitted to the data.

pressure phase and $B_0 = 102(7)$ GPa ($B' = 3.6(3)$) from 16 to 35 GPa in the high pressure phase. $Bi_2Al_4O_9$ ($B_0 = 122(2)$ GPa, $B' = 4.9(3)$) and $Bi_2Mn_4O_{10}$ ($B_0 = 138(2)$ GPa, $B' = 4.2(2)$) show even lower compressibilities (López-de-la Torre *et al* 2009). $\alpha$-$BiB_3O_6$ exhibits a large change of the compressibility between the low pressure phase I (space group $C2$, $B_0 = 38(1)$ GPa) and the high pressure phase II (space group $P1$, $B_0 = 114(10)$ GPa) (Dinnebier *et al* 2009). The bulk modulus of phase I obtained from powder diffraction data (Dinnebier *et al* 2009) is in accordance with the bulk modulus of 34.8 GPa calculated from the elastic constants measured on a single crystal of $\alpha$-$BiB_3O_6$ at ambient conditions (Haussühl *et al* 2006). These examples show that a high compressibility, i.e. a low bulk modulus, at ambient conditions seems to favour the occurrence of a pressure-induced phase transition in LEP

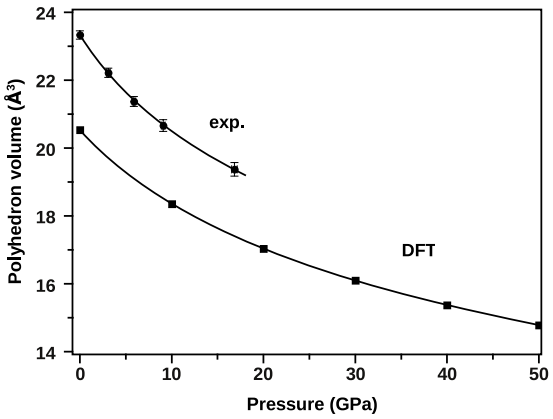


**Figure 5.** Pressure dependence of the $Bi^{[5+2]}O_7$ polyhedron volume from experiment (batch 1) and theory. The solid lines represent the third-order Birch–Murnaghan equations of state which were fitted to the data.

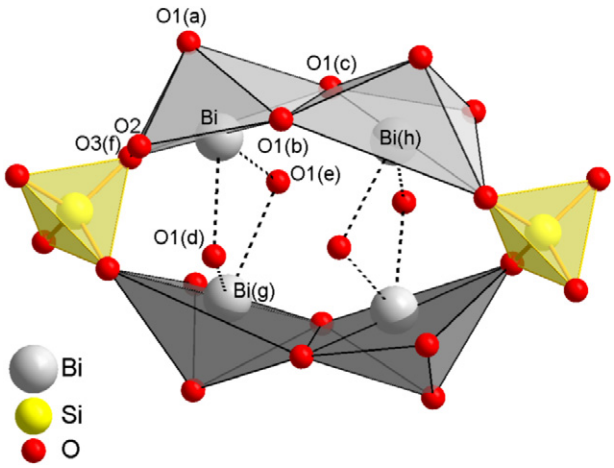


**Figure 6.** In the $Bi_{12}SiO_{20}$ crystal structure $SiO_4$ tetrahedra and $BiO_5$ pyramids form a cavity where the LEPs are localized. The closest contacts between Bi and the two nearest oxygen atoms of the second coordination sphere are indicated as dashed lines.

containing compounds, which in general are characterized by holes in their crystal structures. Thus a phase transition in sillenites could be expected. However, no phase transition was observed in the investigated pressure range, which is rather unusual for such a highly compressible compound. An explanation with respect to specific features of the sillenite structure will be given later.

The overall compressibility can be compared with the compressibility of the cation coordination polyhedra. While the volume of the $SiO_4$-tetrahedra is basically independent of pressure (compare the Si–O3 bond distances in table 4 and figure 8 in section 3.2), the volume of the $Bi^{[5+2]}O_7$ polyhedra decreases significantly with increasing pressure (figure 5). The $Bi^{[5+2]}O_7$ polyhedron volume was calculated (IVTON, Balić-Žunić and Vickovic (1996)) as a function of pressure and its pressure dependence was fitted with a third-order Birch–Murnaghan equation of state, which resulted in the bulk modulus $B_0 = 51(3)$ GPa with pressure derivative $B' = 6.2(7)$. The corresponding values calculated by DFT are $B_0 = 68.2(6)$ GPa and $B' = 4.85(4)$ and here again the overbinding in DFT–LDA calculations leads to an overestimation of $B_0$. The experimental compressibility of the Bi polyhedral volume is thus slightly larger than in $Bi_2Ga_4O_9$ ($B_0 = 61(12)$ GPa) (Friedrich *et al* 2010). In both compounds the bulk modulus of the $BiO_x$ polyhedron is smaller than the bulk modulus of the whole crystal, i.e. the $BiO_x$ polyhedra are compressed more than the crystal, in BSO only slightly more, but in $Bi_2Ga_4O_9$ by a factor of two more. In $Bi_2Ga_4O_9$ the larger compression of the $BiO_x$ polyhedra is compensated by the smaller compression of the two different $GaO_y$ polyhedra with $B_0 = 153.3(5)$ GPa (tetrahedron) and 131(3) GPa (octahedron). In BSO the only other polyhedra are the essentially rigid $SiO_4$ tetrahedra, which occupy a small part of the crystal volume. This explains the rather similar compressibilities of the $BiO_7$ polyhedron and crystal volumes in BSO.

### *3.2. Structural compression*

The crystal structure of $Bi_{12}SiO_{20}$ is composed of $SiO_4$ tetrahedra (site symmetry 23) and distorted $BiO_5\square$ octahedra. The five oxygen atoms approximately form a pyramid, whereas the 'empty' opposite corner of the octahedron is occupied by the $6s^2$ LEP of $Bi^{3+}$ (figure 6). Two pyramids share a common edge and two of these pairs are connected by the $SiO_4$ tetrahedra along the ⟨100⟩ directions, thereby forming a cavity which contains the LEPs. Two adjacent pyramids are symmetrically equivalent due to a two-fold axis in the middle of the shared edge. The second coordination sphere of Bi contains two oxygen atoms (O1(d), O1(e)) at distances of 3.077(7) Å and 3.155(7) Å, respectively, at ambient conditions, indicated by dashed lines in figure 6. These oxygen atoms connect two $Bi^{3+}$ ions across the cavity, i.e. these Bi–O contacts surround the Bi LEPs.

While all the Bi atoms are symmetrically equivalent, three symmetrically distinct oxygen atoms are involved in the coordination and each of the oxygen atoms is part of three different $BiO_5$ polyhedra as shown in figure 7. Part 7(I) (top left) gives an overview of the connectivity and panels 7(II)–(IV) show details of the O1, O2 and O3 environments, respectively. Oxygen atom O1, on a general position, forms the top of the pyramid and simultaneously each end of the shared pyramid edge. Oxygen atom O2 is part of three different $BiO_5$ polyhedra, which are equivalent due to a rotation about a three-fold axis. For O3, also located on a three-fold axis, the situation is similar to O2 with the addition that O3 is a corner of a $SiO_4$ tetrahedron as well.

The pressure dependences of interatomic distances and angles are given in tables 4 and 5 and are shown in figures 8 and 9, respectively. At ambient conditions the distances are in good agreement with the data of Abrahams *et al* (1979). Inspection of the results from the different single-crystal high pressure experiments shows that, due to the limited number of reflections when using Mo K$\alpha$ radiation, the refinement results led to large standard deviations for the coordinates of the atoms and, as a consequence, also for the geometrical parameters characterizing the high pressure structure. In contrast, the shorter wavelength available with synchrotron

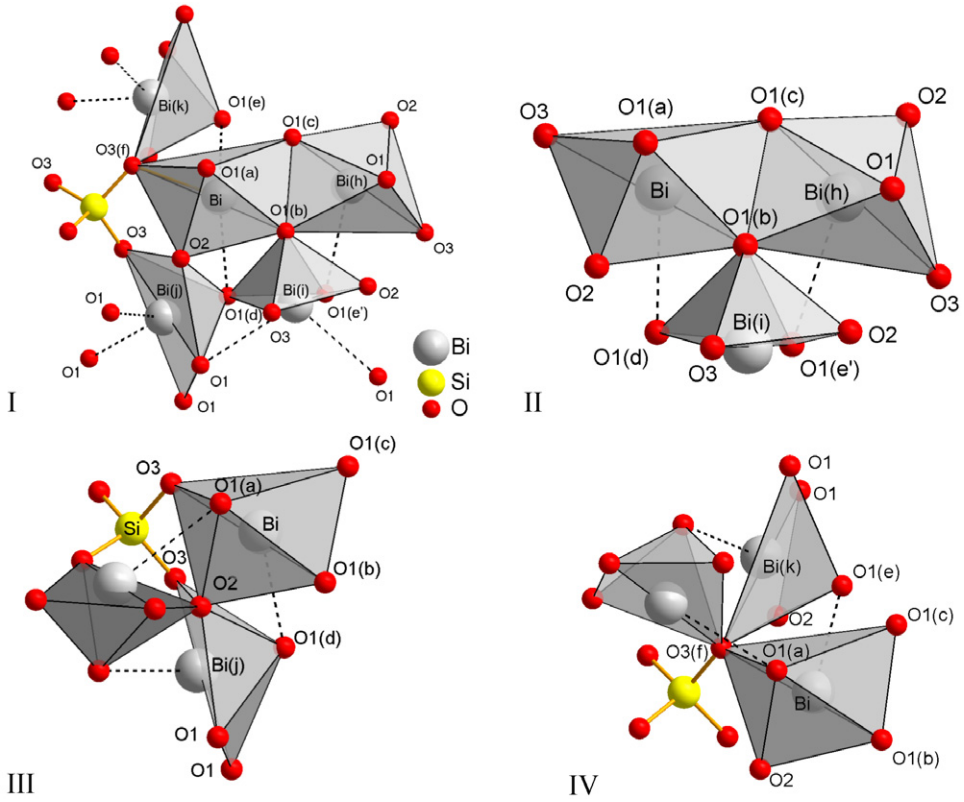


**Figure 7.** Coordination spheres of $Si^{4+}$ and $Bi^{3+}$ ions in the BSO crystal structure with atomic labelling scheme. Dashed lines mark the closest contacts to the nearest non-bonded oxygen neighbours. (I) Overview. (II) O1 coordination. (III) O2 coordination. (IV) O3 coordination.

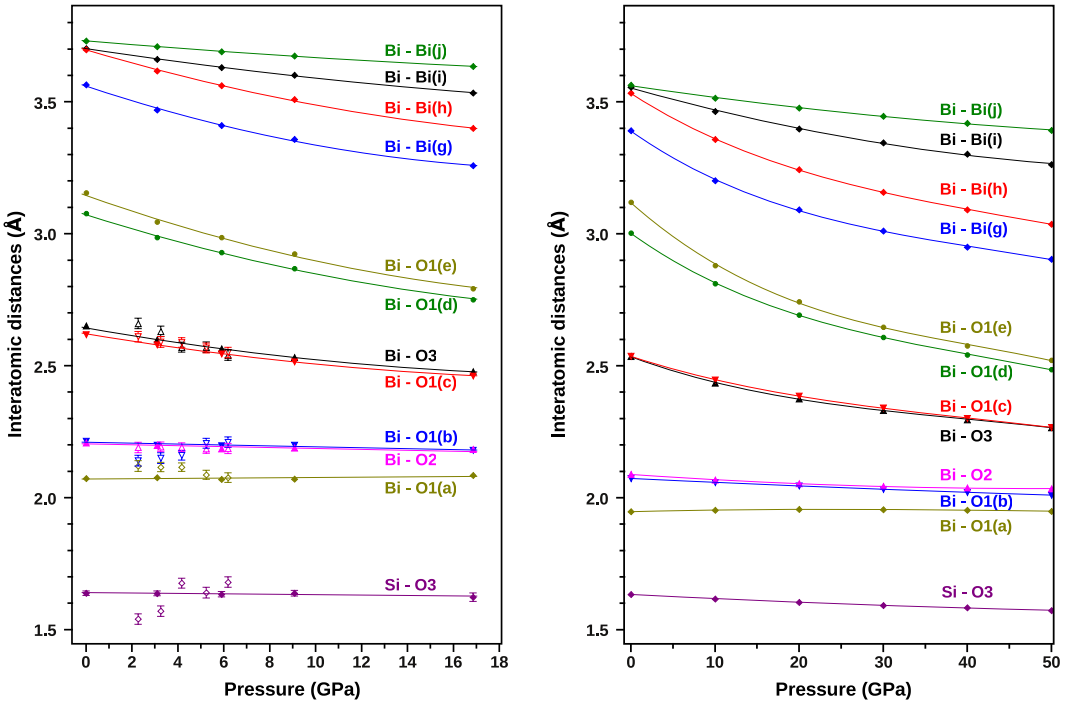


**Figure 8.** Pressure dependences of interatomic distances in BSO. Left: experimental results. Filled symbols mark the high pressure measurements on crystals from batch 1 and open symbols those on crystals from batch 2. Error bars are shown if they exceed the size of the symbols. Right: results from DFT calculations, showing that the compression mechanism does not change up to at least 50 GPa.

radiation reduces absorption effects (here by a factor of three in $\mu$) and increases the accessible fraction of reciprocal space thus improving the parameter to data ratio in the refinement, leading to lower standard deviations of the parameters. Moreover, the higher intensity of the synchrotron radiation allows us to measure more weak reflections, which additionally

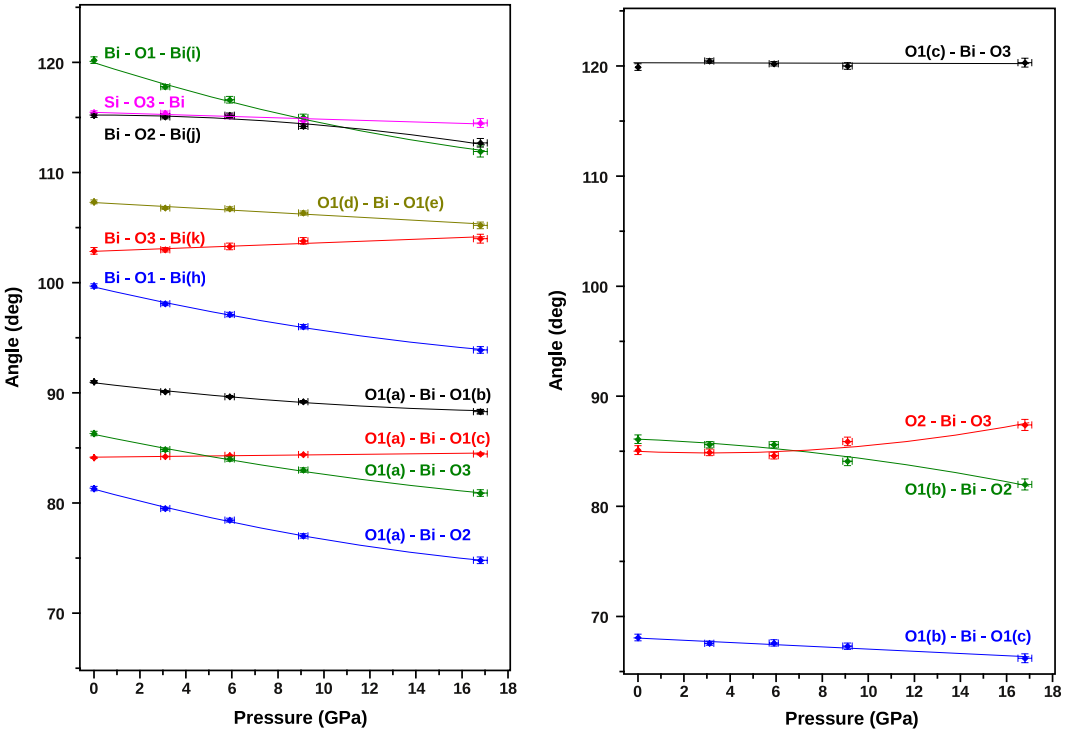


**Figure 9.** Pressure dependences of interatomic angles in BSO (batch 1). Left: bond angles between the top and base plane of the distorted $BiO_5$ pyramid (lower part) and inter-polyhedral angles. Right: bond angles within the base plane of the $BiO_5$ pyramid.

increases the number of reflections. The discussion of the structural parameters at high pressure will therefore refer to the synchrotron data alone.

Due to the use of the local density approximation, the lattice parameters, bond distances and polyhedral volumes derived from DFT calculations are systematically lower than the experimental ones. The pressure evolution of the calculated structural parameters, however, is in good accordance with the experiment and allows a reliable interpretation in the pressure range up to 50 GPa where no experimental data exist.

At high pressure, the regular $SiO_4$ tetrahedra behave as essentially rigid as indicated by the Si–O3 distances, which do not change within the standard deviation up to 16.8 GPa (table 4, figure 8). Such a behaviour was found in several silicates (e.g., Yang *et al* (1997), Miletich *et al* (2000)). In the $BiO_5$ coordination polyhedra the three shortest Bi–O bonds (2.1–2.2 Å), involving atom O1(a), which corresponds to the top of the pyramid, and the two atoms O2 and O1(b), remain essentially constant as a function of pressure. The remaining longer bonds Bi–O1(c) and Bi–O3 (∼2.6 Å) on the other hand are compressed considerably. Distances to the two oxygen atoms of the second coordination sphere (O1(d), O1(e)), which enclose the LEP, exhibit the largest compression. The coordination sphere around Bi thus changes from a pronounced 5 + 2 character towards a sevenfold coordination at higher pressures. These observations correspond well with results on $Bi_2Ga_4O_9$ (Friedrich *et al* 2010) and $Bi_4Ge_3O_{12}$ (Grzechnik 2009). In both compounds the short distances remain constant as a function of pressure, while the longer distances are significantly compressed, indicating a tendency towards higher coordination numbers for $Bi^{3+}$ on pressure increase.

As has been pointed out by Pushkin *et al* (2000), the increase in the number of oxygen atoms bonded to $Bi^{3+}$ in bismuth oxides indicates that the LEP occupies a smaller volume. The effect of pressure on these compounds thus corresponds to a decrease of the stereochemical activity of the LEP. While in BSO the increase of pressure tends to make the Bi–O distances more similar, this is not the case for the corresponding intra-polyhedral angles. The O–Bi–O angles between the oxygen atom O1(a) forming the top of the pyramid and three of the oxygen atoms in the base plane (O1(b), O2, O3) (figure 9 left, lower part) decrease with pressure and their spread is similar at 16.8 GPa and at ambient conditions. The same is true for the angles between the ligands in the base plane (figure 9 right). They range from about 65° to 120° and do not change very much with pressure increase. All this indicates that the effect of pressure on the coordination polyhedron of $Bi^{3+}$ is mainly to increase the coordination number to seven but leaves the highly irregular shape nearly unchanged.

The by far shortest Bi–Bi distance at ambient conditions is Bi–Bi(g) (3.56 Å) in the direction of the LEPs, followed by three larger and nearly equal distances of 3.70–3.74 Å. On compression, however, the Bi–Bi(h) distance perpendicular to the LEP decreases by the same amount as the Bi–Bi(g) distance in the direction of the LEPs (figures 6 and 8). Both distances are located within one cavity which implies that the cavity as a whole is compressed nearly isotropically. If one takes into account that the $SiO_4$ tetrahedra remain nearly unchanged by pressure, the consequence is a considerable bending of the $BiO_5$ pyramids along their shared edge. This is reflected in the large reduction of the inter-pyramidal angles Bi–O1–Bi(h) by 5.9° and Bi–O1–Bi(i) by 7.7° between ambient

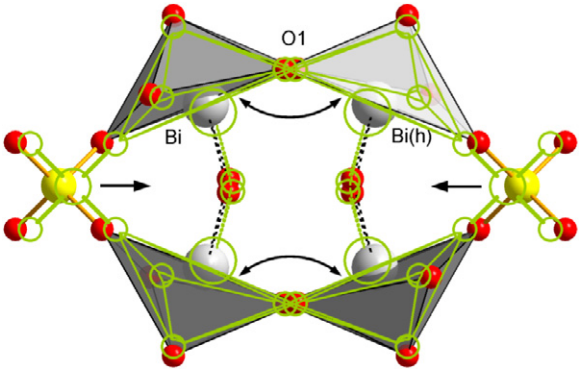


**Figure 10.** Overlay of the crystal structures at ambient conditions (shaded areas, in colour online) and at 16.8 GPa (grey lines, in green online).

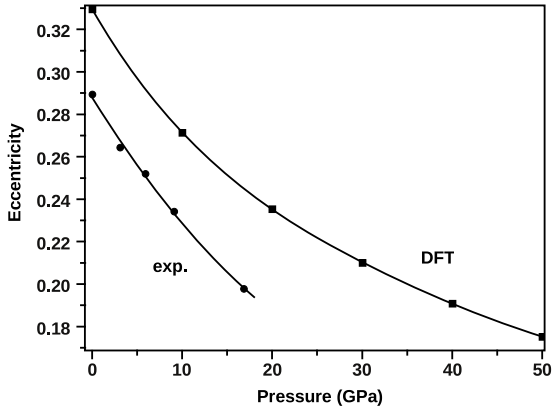


**Figure 11.** Pressure dependence of the eccentricity of the $Bi^{3+}$ cation from experiment and theory (DFT).

conditions and 16.8 GPa (figure 9 left), whereas the inter-pyramidal angles with centre at O2 or O3 change only by 3.0° and 1.3°, respectively, and the Si–O3–Bi angle by 1.1°. Even the O1(e)–Bi–O1(e) angle (figures 6 and 9 left), which encloses the LEP, is reduced only by 2.0°. Figure 10 shows an overlay of the crystal structures (one cage) at ambient pressure (shaded polyhedra) and 16.8 GPa (grey lines, green online). On increasing pressure the $SiO_4$ tetrahedra move closer together and the $BiO_5$ pyramids of Bi and Bi(h) are tilted at O1. The large Bi–O1–Bi(i) tilt angle corresponds to a relative tilt of two $BiO_5$ polyhedra which belong to different cages (figure 7(II)). One might expect that such an atom group as shown in figure 10 should be compressed essentially in direction of the LEPs (vertical direction) in order to reduce the volume of empty space. Such a compression is prevented, however, in the sillenite structure due to the fact that these groups are oriented in three different, mutually perpendicular directions. This is thought to increase the stability of the sillenite structure at high pressure.

A useful measure for the stereochemical activity of the LEP is the eccentricity of the coordination polyhedra around the cation (Balić-Žunić and Makovicky 1996). This parameter reflects the regularity of the coordination polyhedron and is defined as the distance between cation position and centroid, divided by the mean distance of the ligands from the centroid, where the centroid of coordination is the point with the minimum variance of distances to all ligands (Balić-Žunić and Makovicky 1996). The cation eccentricity $e$ of the $Bi^{[5+2]}O_7$ polyhedron was calculated as a function of pressure using IVTON (Balić-Žunić and Vickovic 1996). It decreases with increasing pressure from $e = 0.289$ to 0.198 at 16.8 GPa as is shown in figure 11, indicating a reduction of the stereochemical activity of the LEP. In $Bi_2Ga_4O_9$ (Friedrich *et al* 2010) the Bi cation eccentricity ($e = 0.281$ at ambient conditions) is comparable, but the reduction with pressure in the low pressure phase ($e = 0.235$ at 14.9 GPa) is less than in BSO. The eccentricities in these oxides are much larger then those in some sulfides of the LEP ions $Bi^{3+}$, $Sb^{3+}$ and $Pb^{2+}$. At ambient conditions $e \approx 0.15$ in bismuthinite, $Bi_2S_3$ (Lundegaard *et al* 2005), $0.19 < e < 0.23$ in stibnite, $Sb_2S_3$ (Lundegaard *et al* 2003), $0.08 < e < 0.12$ in galenobismutite, $PbBi_2S_4$ (Olsen *et al* 2007), $0.04 < e < 0.10$ in lillianite, $Pb_3Bi_2S_6$ (Olsen *et al* 2008), and $0 < e < 0.228$ in heyrovskyite, $Pb_6Bi_2S_9$ (Olsen *et al* 2010). In the first three compounds the eccentricities decrease by 0.1 or less in the pressure range up to 10 GPa. In comparison, the eccentricity of the Bi cation which is also reduced by 0.1, and hence the stereochemical activity of the LEP, remains rather high in BSO up to 16.8 GPa. Lillianite and heyrovskyite, on the other hand, are not directly comparable, as the eccentricities for the various cation sites in the structures increase considerably (up to $e = 0.57$) after undergoing first-order phase transitions to their respective high pressure polymorphs. The eccentricities of BSO deduced from the density functional calculations confirm the trend of a continuously decreasing stereochemical activity of the $Bi^{3+}$ LEP up to 50 GPa.

### 3.3. Vibrational properties

Raman spectra of sillenites at ambient pressure have been extensively studied and discussed by Venugopalan and Ramdas (1972), Mihailova *et al* (1997, 1999) and Burkov *et al* (2001). Group-theory analysis predicts that there are 8A (totally symmetric), 8E (doubly degenerate), and 24F (triply degenerate) zone-centre optical phonons. The A, E, and F modes are Raman active, while the latter are also infrared active. Due to the lack of an inversion centre long-range polarization fields are expected to split the F modes into longitudinal-optic (LO) and transverse-optic (TO) phonons, with the former shifted to a higher frequency (Venugopalan and Ramdas 1972, Burkov *et al* 2001). Such a splitting has been observed in the Raman spectra of BSO and BGO at 15 K by Venugopalan and Ramdas (1972), but not at ambient conditions.

The pressure dependences of the observed and calculated bands of BSO and their symmetry assignments are shown in figure 12. The values at ambient pressure are listed in table 6, whereas the Raman shifts measured at high pressures and the calculated Raman shifts at 10, 20, 30, 40 and 50 GPa can be found in supplementary tables (available at stacks.iop.org/JPhysCM/22/505401/mmedia). The numbering of modes has been adopted from Mihailova *et al* (1999). As many of the observed bands are not well resolved at ambient temperature, the frequencies obtained at 15 K (Venugopalan and Ramdas

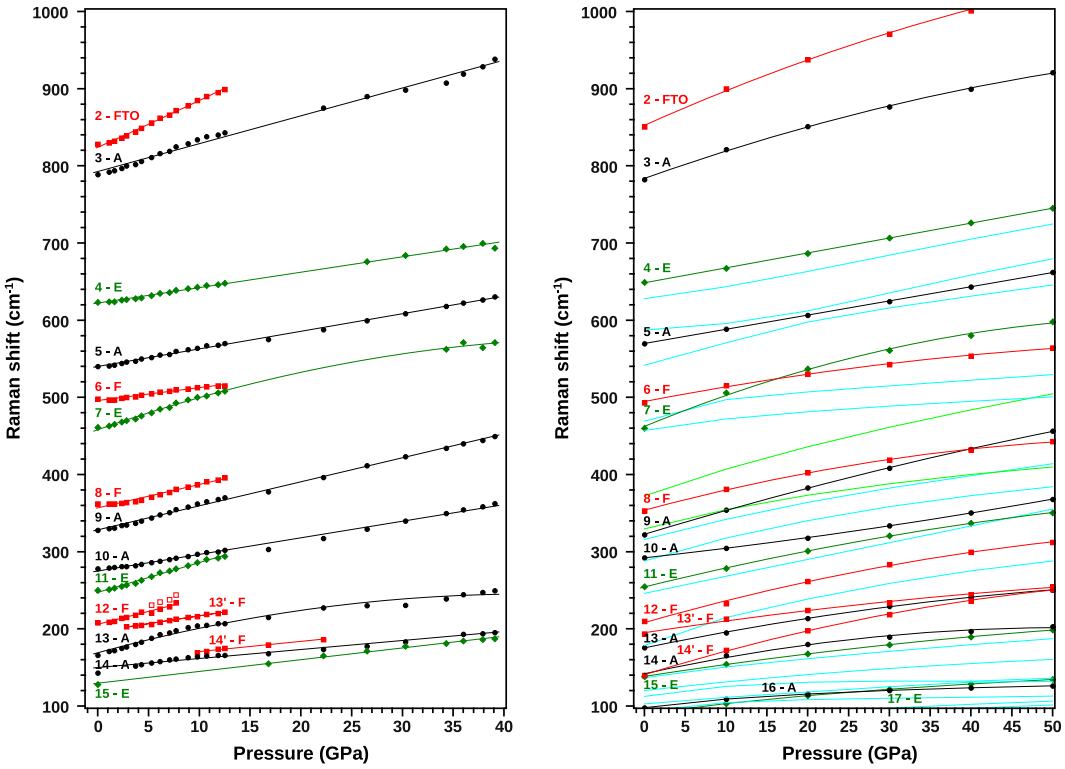


**Figure 12.** Pressure dependence of the Raman bands. The lines connecting data points represent linear (in some cases quadratic) fits to the data. Symbols (and online colours) are: circles (black) for A modes, diamonds (green) for E modes and squares (red) for F modes. Left: experimental results from single crystal and powder data. Right: theoretical results from DFPT calculations. The grey lines (green or cyan in the online version) represent calculated modes which were not measured or not resolved at ambient temperature. Most of these are F modes (cyan) apart from two E modes (light green) between 330 and 380 $cm^{-1}$.

1972) are included in table 6. There is an excellent agreement with the calculated frequencies at 0 GPa. Only a few modes (no. 2, 4, 5, 10, 15) show frequency differences (calc–obs) of 10 $cm^{-1}$ or larger and only three of these bands (no. 5, 10, 15) have strong intensities. All the bands shift to higher energies on compression. This effect is considerably larger than the slight temperature shifts reported between 15 and 300 K. Comparison of the pressure evolution of the observed and calculated bands enabled us to unambiguously assign the modes to the observed frequencies up to 40 GPa. No anomalies in the evolution of the Raman spectra can be detected that would indicate a structural phase transition.

Apart from the F(TO) and F(LO) phonons (no. 12) at about 206 $cm^{-1}$ above 5 GPa, no other TO and LO modes become resolved at high pressures. The two bands appearing at about 3 GPa around 200 $cm^{-1}$ (no. 13′) and at about 10 GPa around 170 $cm^{-1}$ (no. 14′) could be assigned to F modes by comparison with the calculated Raman shifts (figure 12). The corresponding lines at ambient pressure are not resolved into LO and TO down to 15 K (Venugopalan and Ramdas 1972). A correlation of the Raman modes 3-A, 6-F, 7-E and 8-F with internal vibrations of the $SiO_4$ tetrahedra was suggested by Venugopalan and Ramdas (1972) on the basis of calculated normal-mode frequencies of the $SiO_4$ unit and the approximation that the zone-centre phonons of sillenites may be divided into those originating from the normal modes of the tightly bound $MO_4$ unit and those modes where the entire $MO_4$ unit vibrates against the other atoms in the crystal. Mihailova *et al* (1997, 1999) provided detailed assignments of modes to certain Bi–O and $MO_4$ vibrations for pure BSO, doped BSO with 14 different ions on the $M$ site and (Si, Mn) mixed sillenite crystals, based on frequency shifts calculated from a small cluster and the comparison of the frequency shifts due to different ions on the tetrahedral site. According to these investigations, the lines 1-FLO, 2-FTO, 3-A and partly 6-F, 20-F are correlated with internal modes of the $SiO_4$ tetrahedra, whereas all other modes represent Bi–O vibrations. The strongest lines in the spectra are the A modes in the frequency range from about 150 to 700 $cm^{-1}$ (modes no. 5, 9, 10, 14), which are assigned to Bi–O ‘breathing’ modes and the E mode no. 15 at about 128 $cm^{-1}$ which is assigned to Bi and O2 vibrations elongating the cluster.

The pressure dependence of the observed Raman bands can be correlated with the pressure dependence of the unit cell volume through a microscopic mode-Grüneisen parameter ($\gamma_i$) at constant temperature ($T = 298$ K),

$$\gamma_i = (\partial \ln \nu_i / \partial \ln V) = (B_0/\nu_{i0})(\partial \nu_i / \partial p),$$

where $\nu_i$ is the wavenumber of the $i$th vibrational mode ($cm^{-1}$), $V$ is the corresponding unit cell volume ($Å^3$) and $B_0$ the bulk modulus at zero pressure (GPa), and $p$ is the corresponding pressure (GPa). The resulting values of the $\gamma_i$ parameters from experiment and theory, using $B_0 = 63$ GPa, are given in table 6. They agree well in most cases. It

**Table 6.** Raman shifts of BSO at ambient conditions from experiment and theory with calculated microscopic mode-Grüneisen parameters $\gamma_i$ (using $B_0 = 63$ GPa). Included are the Raman shifts and mode assignments from Venugopalan and Ramdas (1972) at 15 K.

| | Experiment at 1 bar | | | Theory (DFPT) at 0 GPa | | Venugopalan and Ramdas (1972) at 15 K | |
|---|---|---|---|---|---|---|---|
| Nr. | Shift ($cm^{-1}$) | $\gamma_i$ | Mode | Shift ($cm^{-1}$) | $\gamma_i$ | Shift ($cm^{-1}$) | Mode |
| 20 | | | F | 43 | | 44 | TO + LO |
| | | | | | | 46 | LO |
| | | | F | 52 | | 51 | TO + LO |
| | | | | | | 54 | LO |
| 19 | | | F | 60 | | 58 | TO + LO |
| | | | A | 67 | | | |
| 18 | | | E | 70 | | 68 | E |
| 17 | | | E | 90 | | 88 | E |
| | | | F | 93 | | 89 | TO + LO |
| 16 | | | A | 98 | | 92 | A |
| | | | F | 103 | | 99 | TO |
| | | | | | | 101 | LO |
| | | | F | 113 | | 106 | TO + LO |
| | | | | | | 112 | LO |
| | | | F | 120 | | 114 | F or TO |
| | | | | | | 118 | F |
| | | | F | 137 | | | |
| 15 | 128 | 0.74 | E | 138 | 0.74 | 132 | E |
| 14 | 143 | 0.49 | A | 140 | 1.03 | 149 | A |
| 14′ | | 0.53 | F | 140 | 1.47 | 136 | TO + LO |
| | | | | | | 167 | LO |
| 13 | 166 | 1.34 | A | 176 | 0.79 | 171 | A |
| | | | F | 178 | | 174 | TO |
| | | | | | | 181 | LO |
| | | | | | | 185 | LO |
| 13’ | | 0.65 | F | 194 | 0.52 | 196 | F |
| 12 | 208 | 1.02 | F | 210 | 0.91 | 209 | TO |
| | | | | | | 213 | LO |
| | | | F | 246 | | 238 | F or TO |
| 11 | 250 | 0.98 | E | 255 | 0.64 | 252 | E |
| | | | F | 288 | | | |
| 10 | 278 | 0.49 | A | 292 | 0.25 | 282 | A |
| | | | F | 316 | | | |
| 9 | 328 | 0.60 | A | 322 | 0.62 | 331 | A |
| | | | E | 330 | | | |
| | | | F | 353 | | 352 | TO + LO |
| 8 | 362 | 0.53 | F | 369 | 0.51 | 367 | TO + LO |
| | | | E | 372 | | 373 | E |
| | | | F | 457 | | | |
| 7 | 461 | 0.63 | E | 460 | 0.59 | 464 | E |
| | | | F | 469 | | 469 | F |
| 6 | 498 | 0.21 | F | 493 | 0.26 | 496 | TO + LO |
| | | | F | 542 | | 509 | TO + LO |
| 5 | 540 | 0.27 | A | 570 | 0.20 | 546 | A |
| | | | F | 587 | | | |
| | | | F | 628 | | | |
| 4 | 623 | 0.20 | E | 649 | 0.19 | 626 | E |
| 3 | 789 | 0.29 | A | 782 | 0.30 | 785 | A |
| 2 | 828 | 0.47 | F | 851 | 0.35 | 827 | TO |
| 1 | | | | | | 841 | LO |

is clearly seen that the mode-Grüneisen parameters for the $SiO_4$ internal modes (no. 2, 3, 6) in general are smaller ($0.21 < \gamma < 0.47$) than for the modes derived from the oscillations of the (Bi, O) sublattice ($0.20 < \gamma < 1.34$). This is consistent with the compressibility mechanism as obtained from the x-ray investigations, in which the changes in the Bi–O interatomic distances account for nearly all of the compressibility, while the $SiO_4$ units are essentially rigid. In $Bi_2Ga_4O_9$ (Friedrich *et al* 2010) the $GaO_x$ polyhedra are less compressible than the $BiO_6$ octahedra and the mode-Grüneisen parameters associated with the Ga–O vibrations ($0.45 < \gamma < 1.25$) are slightly larger than those for the Bi–O modes ($0.01 < \gamma < 0.94$). In $Bi_2Ga_4O_9$, however, the Bi ion is located in a symmetry-constrained position. There is no simple correlation between the bulk modulus of a polyhedron and the mode-Grüneisen parameters of the internal vibrational modes of this polyhedron, but the specific binding conditions have to be considered.

## 4. Conclusions

The cubic crystal structure of BSO exhibits a remarkable pressure stability despite its high compressibility. Single-crystal x-ray diffraction up to 23 GPa and *ab initio* calculations of the crystal structure by density functional theory up to 50 GPa show no indication of a structural phase transition. As the $SiO_4$ tetrahedra are essentially rigid, nearly all compression is due to a volume decrease of the $BiO_x$ polyhedra. The Bi coordination number increases from 5 + 2 to 7 and the stereoactivity of the LEP is reduced as indicated by the pressure-induced decrease of the $Bi^{3+}$ cation eccentricity. As the spread of the bond angles is much larger than their changes with pressure, the $BiO_x$ polyhedron retains its irregular shape. The largest changes of interatomic angles observed during pressure increase are changes of tilt angles between adjacent $BiO_x$ polyhedra. These tilts are necessary to fit the differently compressed interconnected polyhedra into the isotropically compressed unit cell. The extreme stability of the sillenite crystal structure is closely related to the high symmetry which prevents a preferred compression of the cavities in the direction of the LEPs.

The vibrational properties support these results. The Raman shifts and the mode-Grüneisen parameters from experiment and theory agree well and allow us to confidently extrapolate our findings to much higher pressures than we have reached experimentally.

## Acknowledgments

This research was supported by Deutsche Forschungsgemeinschaft (DFG), Germany, within the Project HA 5137/3-1. Portions of this research were carried out at the light source DORIS III at DESY. DESY is a member of the Helmholtz Association (HGF). We would like to thank M Tolkiehn for assistance in using beamline D3 and HASYLAB for financial support. A Friedrich thanks the DFG (projects WI 1232/25-1 and FR 2491/2-1 within SPP-1236) for support and W Morgenroth thanks the BMBF (project 05KS7RF1) for support. A Grzechnik and K Friese acknowledge technical and financial support from the University of the Basque Country (SGIker), the Gobierno Vasco, and the Ministerio de Ciencia e Innovación (FIS2008-03834). L Wiehl thanks B Mihailova for the assistance with the pressure measurements at the University of Hamburg. Some of the single crystals of BSO were synthesized and provided for this study by V Marinova.

## References

Abrahams S C, Bernstein J L and Svensson C 1979 *J. Chem. Phys.* **71** 788–92
Ahuja R 2003 *Phys. Status Solidi* b **235** 341–7
Angel R J 2001 *EOS–FIT Version 5.2* (Blacksburg, USA: Virginia Tech)
Angel R J 2004 *J. Appl. Crystallogr.* **37** 486–92
Arora A K, Yagi T, Miyajima N and Gopalakrishnan R 2004 *J. Phys.: Condens. Matter* **16** 8117–30
Atou T, Faqir H, Kikuchi M, Chiba H and Syono Y 1998 *Mater. Res. Bull.* **33** 289–92
Baade T, Kiessling A and Kowarschik R 2001 *J. Opt. A: Pure Appl. Opt.* **3** 250–4
Balić-Žunić T and Makovicky E 1996 *Acta Crystallogr.* B **52** 78–81
Balić-Žunić T and Vickovic I 1996 *J. Appl. Crystallogr.* **29** 305–6
Birch F 1947 *Phys. Rev.* **11** 809–24
Boehler R 2006 *Rev. Sci. Instrum.* **77** 115103
Boehler R and de Hantsetter K 2004 *High Press. Res.* **24** 391–6
Burkov V I, Gorelik V S, Egorysheva A V and Kargin Y F 2001 *J. Russ. Laser Res.* **22** 243–67
Buse K 1997 *Appl. Phys.* B **64** 391–407
Chattopadhyay T, von Schnering H G, Grosshans W A and Holzapfel W B 1986 *Physica* B + C **139** 356–60
Clark S J, Segall M D, Pickard C J, Hasnip P J, Probert M I J, Refson K and Payne M C 2005 *Z. Kristallogr.* **220** 567–70
Coppens P 1970 *Crystallographic Computing* ed F R Ahmed, S Hall and C P Huber (Copenhagen: Munksgaard) pp 255–70
Dinnebier R E, Carlson S, Hanfland M and Jansen M 2003 *Am. Mineral.* **88** 996–1002
Dinnebier R E, Hinrichsen B, Lennie A and Jansen M 2009 *Acta Crystallogr.* B **65** 1–10
Eichhorn K 1978 *AVSORT* HASYLAB/DESY Hamburg, Germany
Eichhorn K 1987 *REDUCE* HASYLAB/DESY Hamburg, Germany
Filippov V N, Starodumov A N, Barmenkov Y O and Makarov V V 2000 *Appl. Opt.* **39** 1389–93
Friedrich A, Juarez-Arellano E, Haussühl E, Boehler R, Winkler B, Wiehl L, Morgenroth W, Burianek M and Mühlberg M 2010 *Acta Crystallogr.* B **66** 323–37
Georges M P, Scauflaire V S and Lemaire P C 2001 *Appl. Phys.* B **72** 761–5
Gospodinov M, Haussühl S, Sveshtarov P, Tassev V and Petkov N 1988 *Bulg. J. Phys.* **15** 140–3
Grzechnik A 2009 *Acta Crystallogr.* C **65** i63–5
Grzechnik A and Friese K 2010 *J. Phys.: Condens. Matter* **22** 095402
Haussühl S, Bohatý L and Becker P 2006 *Appl. Phys.* A **82** 495–502
Kaneko T, Tsuji T, Ohdou J, Otsubo M, Honda C, Kubozono T, Ueda Y and Oguro Y 1999 *Electr. Eng. Japan* **128** 84–93
Klotz S, Chervin J C, Munsch P and LeMarchand G 2009 *J. Phys. D: Appl. Phys.* **42** 075413
Li X, Yang J, Yang J, Chang S, Liu J and Hu W 2007 *Appl. Opt.* **46** 3774–9
López-de-la Torre L, Friedrich A, Juarez-Arellano E A, Winkler B, Wilson D J, Bayarjargal L, Hanfland M, Burianek M, Mühlberg M and Schneider H 2009 *J. Solid State Chem.* **182** 767–77
Lu Y H, Yeo T S, Kooi P S, Pan J C and Zhang C B 2000 *Microw. Opt. Technol. Lett.* **24** 263–7
Lundegaard L F, Makovicky E, Boffa-Ballaran T and Balić-Žunić T 2005 *Phys. Chem. Miner.* **32** 578–84
Lundegaard L F, Miletich R, Balić-Žunić T and Makovicky E 2003 *Phys. Chem. Miner.* **30** 463–8
Mao H K, Bell P M, Shaner J W and Steinberg D J 1978 *J. Appl. Phys.* **49** 3276–83
Mao H K, Xu J and Bell P M 1986 *J. Geophys. Res.* B **91** 4673–6
Meng J F, Dobal P S, Katiyar R S and Zou G T 1998 *J. Raman Spectrosc.* **29** 1003–8
Mihailova B, Gospodinov M and Konstantinov L 1999 *J. Phys. Chem. Solids* **60** 1821–7
Mihailova B, Konstantinov L, Petrova D and Gospodinov M 1997 *Solid State Commun.* **102** 441–4
Miletich R, Allan D R and Kuhs W F 2000 *High-Temperature and High-Pressure Crystal Chemistry* (*Rev. Mineral. Geochem.* vol 41) ed R M Hazen and R T Downs (Washington, DC: The Mineralogical Society of America and the Geochemical Society) pp 445–520
Monkhorst H J and Pack J D 1976 *Phys. Rev.* B **13** 5188–92
Neov S, Marinova V, Reehuis M and Sonntag R 2002 *Appl. Phys.* A **74** (Suppl.) S1016–8
Olsen L A, Balić-Žunić T and Makovicky E 2008 *Inorg. Chem.* **47** 6756–62

Olsen L A, Balić-Žunić T, Makovicky E, Ullrich A and Miletich R 2007 *Phys. Chem. Miner.* **34** 467–75
Olsen L A, Friese K, Makovicky E, Balić-Žunić T, Morgenroth W and Grzechnik A 2010 *Phys. Chem. Miner.* at press
Petricek V, Dusek M and Palatinus L 2006 *Jana2006. The Crystallographic Computing System* Institute of Physics Prague, Czech Republic
Piermarini G J, Block S, Barnett J D and Forman R A 1975 *J. Appl. Phys.* **46** 2774–80
Porezag D and Pederson M R 1996 *Phys. Rev.* B **54** 7830–6
Pushkin D V, Sokolova E A and Serezhkin V N 2000 *Russ. J. Coord. Chem.* **26** 1–5
Radaev S F, Simonov V I and Kargin Y F 1992 *Acta Crystallogr.* B **48** 604–9
Ravindran T R, Arora A K and Gopalakrishnan R 2002 *J. Phys.: Condens. Matter* **14** 6579–89
Refson K, Tulip P R and Clark S J 2006 *Phys. Rev.* B **73** 155114
Seshadri R 2006 *Solid State Sci.* **8** 259–66
Sheldrick G M 1997 *SHELXL97-2. Program for Crystal Structure Refinement* Göttingen, Germany
Sillen L G 1938 *Ark. Kemi Mineral. Geol.* A **12** 1–15
Skorikov V M, Kargin Y F, Egorysheva A V, Volkov V V and Gospodinov M 2005 *Inorg. Mater.* **41** (suppl. 1) S24–46
STOE and CIE GmbH 2006 *X-Area; MainMenu Version 1.39* Darmstadt, Germany
Syassen K 2005 *DATLAB Version 1.38 MPI/FKF* Stuttgart, Germany
Temple P A and Hathaway C E 1973 *Phys. Rev.* B **7** 3685–97
van den Tempel C M M 1993 *Appl. Opt.* **32** 4869–74
Venugopalan S and Ramdas A K 1972 *Phys. Rev.* B **5** 4065–79
Wells A F (ed) 1984 *Structural Inorganic Chemistry* 5th edn (Oxford: Oxford University Press) pp 890–1
Winkler B, Milman V and Lee M H 1998 *J. Chem. Phys.* **108** 5506–9
Yang H, Hazen R M, Finger L W, Prewitt C T and Downs R T 1997 *Phys. Chem. Miner.* **25** 39–47